AIAA AVIATION Forum
August 2-6, 2021, VIRTUAL EVENT
AIAA AVIATION 2021 FORUM

10.2514/6.2021-2919

High-Speed, Short-Pulse-Duration Light Source for Digital Inline Holographic Imaging of Multiphase Flow Fields

A. Dworzanczyk* and N. J. Parziale†
Stevens Institute of Technology, Hoboken, NJ 07030, USA

In preparation for ballistic-range testing, we develop a Digital Inline Holography (DIH) capability as applied to a simple jet flow in the lab. To address the challenges specific to a ballistic range, we devise a laser diode light source for DIH which may be spatially filtered and pulsed at high repetition rates with very short exposure times. We use this light source to record holograms of a droplet falling into a jet flow and process them with HoloSand.

I. Nomenclature

A_r	=	reconstructed amplitude
γ	=	surface tension
D_T	=	Tenengrad depth
d_{drop}	=	drop diameter
d_0	=	orifice diameter
E	=	reconstructed complex amplitude
E_r^*	=	conjugate reference wave
$\mathcal{F}$	=	Fourier transform
g	=	Rayleigh-Sommerfeld diffraction kernel
I_0	=	hologram intensity
κ	=	wave number
L	=	reference length
λ	=	wavelength
μ	=	viscosity
Oh	=	Ohnesorge number
ρ	=	density
$S_{\text{x,y}}$	=	Sobel kernel
S_W	=	sharpness
T	=	Tenengrad Operator
$\mathcal{T}$	=	Thresholding Operation
t	=	threshold
v	=	flow velocity
We	=	Weber number
ξ	=	Edge-finding Operation
z	=	distance between detector and object planes

II. Introduction

Digital Inline Holography (DIH) is an imaging technique for three-dimensional flow fields that reconstructs the location and shape of an object in the field from the interference pattern (or hologram) generated when a plane or spherical wave of coherent light illuminates it [1]. As 3-D information coded in a digital hologram can be recorded in one image, this technique can be used with high-speed cameras to perform time-resolved 3-D reconstructions of high-speed phenomena. Improvements in computer technology and digital imaging have allowed this technique to progress substantially in the past several decades with much work done in experimental mechanics, biology, and fluid dynamics.

*Graduate Student, Mechanical Engineering, Castle Point on Hudson, Hoboken, NJ 07030.
†Assistant Professor, Mechanical Engineering, Castle Point on Hudson, Hoboken, New Jersey, 07030, AIAA Senior Member.

Gao et al. [2] and Guildenbecher et al. [3] developed a set of MATLAB functions to process digital holograms called Sandia Particle Holography Processor or HoloSand [4]. Following their work, we can write the reconstructed complex amplitude, E, as

$$E(x, y, z) = \left[I_0(x, y)E_r^*(x, y)\right] \otimes g(x, y, z), \tag{1}$$

where $I_0(x, y, z)$, E_r^*, $\otimes$, and $g(x, y, z)$ are the the hologram intensity, conjugate reference wave, convolution operator, and the Rayleigh–Sommerfeld diffraction kernel, respectively. Guildenbecher et al. [3] writes this operator as

$$g(x, y, z) = \exp\left(j\kappa\sqrt{x^2 + y^2 + z^2)}\right) / (j\lambda)\sqrt{x^2 + y^2 + z^2}, \tag{2}$$

where λ, κ, and z are the laser wavelength, wave number, and propagation distance from the hologram. Then, Eq. 1 is solved with the Fourier transform as

$$E(x, y, z) = \mathcal{F}^{-1}\left\{\mathcal{F}\left\{I_0(x, y)\right\} \cdot G(f_x, f_y; z)\right\}, \tag{3}$$

where $\mathcal{F}$ and $\mathcal{F}^{-1}$ are the Fourier transform and inverse Fourier transform. $G(f_x, f_y; z)$ is the Fourier transform of Eq. 2,

$$G(f_x, f_y; z) = \exp\left[j\kappa z\sqrt{1 - \lambda^2 f_x^2 - \lambda^2 f_y^2}\right], \tag{4}$$

where f_x and f_y are the transverse spatial frequencies, and also noting that E_r^* is a plane reference wave with unit amplitude. This mathematical framework is used in MATLAB functions to calculate a range of possible distances between the sensor and object planes for every pixel of a hologram; these scripts seek to find the distance where the image intensity is minimized and the Tenengrad operator is maximized. Reconstructed image intensity is expected to be minimized immediately behind the object blocking the incoming light source; locations further from the object will have a greater intensity because of light diffraction around the edges of the object. The Tenengrad operator is a measure of image focus and the gradient of light intensity across a region; its maxima indicate the locations of sharp edges. This hybrid method of particle reconstruction, combining edge-detection and intensity-minimization, was compared with six other methods (the Laplacian, Correlation Coefficient, Variance, Minimum Intensity, Minimum Edge Intensity, and Integrated Gradient methods) to determine which could most accurately track and size particles. The hybrid method was among the most accurate, and, alone among the studied techniques, could be used for automatic segmentation, that is, identifying distinct particles in the same hologram.

Guildenbecher et al. [5] used the DIH reconstruction functions they developed to study the breakup of a spherical drop of ethanol subjected to a step change of relative gas velocity. Drops of ethanol 2.5 mm in diameter were subjected to air flows of 10.5 to 21.5 m/s, conditions corresponding to Weber numbers between 14 and 55. At lower Weber numbers, the droplets were observed to break up through bag breakup morphology. That is, the drops flattened and inflated into thin bags of liquid, open in the direction from which air flowed. The thin bag shatters, leaving a toroidal thick section around the rim that itself subsequently fragments. The holography techniques employed in these experiments allowed for measurement of approximately 10,000 fragments per droplet, a significant improvement on the several hundred observed per droplet in earlier studies and greatly reducing uncertainty in fragment size distribution. Such an improvement could be useful at higher Weber numbers, where droplet breakup involves flattening of the droplet and liquid stripping from the edges of each flattened droplet, similar to that discussed by Reinecke [6].

The objective of this work is to develop a DIH capability as applied to a simple jet flow in the lab (as in [5], for example) that would be appropriate for ballistic-range testing. Unique challenges to the ballistic-range testing testing environment are high-intensity luminosity from the projectile, strong refractive effects from shock waves, and extreme velocities. To address these, we devise a laser diode light source for DIH which may be spatially filtered and pulsed at high repetition rates with very short exposure times. We use this light source to record holograms of a droplet falling into a jet flow and process them with HoloSand.

III. Facility and Experimental Setup

A schematic drawing of the experimental setup is provided in Fig. 1. Isopropanol droplets are generated by a Microfab ABL 120 dispenser. This dispenser, with an orifice diameter of 120 microns and pointed in the -Y direction, is fed by a syringe pump at a constant volumetric flow rate, and controlled by a function generator amplified by a Thorlabs

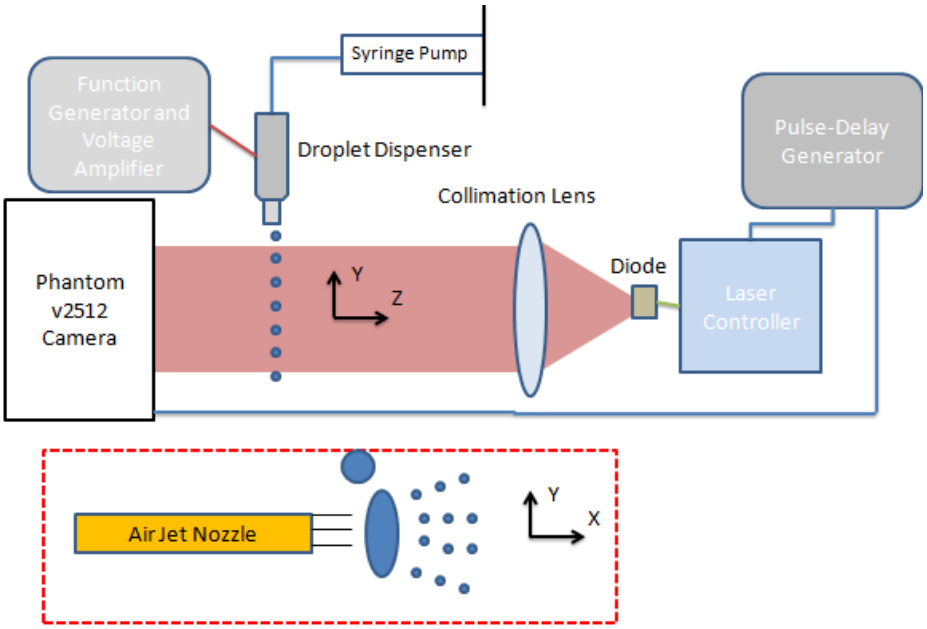

Fig. 1 Schematic diagram of experimental setup. Phantom camera controls frequency of pulse-delay generator, which provides pulses to laser controller. Diode produces red laser beam collimated by convex lens, which illuminates isopropanol droplets produced by dispenser. Inset window, outlined in red dashed lines, shows air jet pointed in +X direction, and expected drop breakup behavior.

BPA100 piezo amplifier at 10 V. The Microfab ABL 120 droplet dispenser is a piezoelectric device that induces a surface disturbance in the stream of liquid. This disturbance amplifies through Laplace pressure until, at some distance from the dispenser orifice, the stream breaks into evenly-spaced near-spherical droplets. This process was documented by Shimisaki and Taniguchi in their 2011 report on droplet formation in liquid metal streams [7]. If one perturbs the liquid stream at an optimal frequency, f, related to the velocity, v as $f = v/\lambda$, the optimal droplet separation distance, λ is given by

$$\lambda = \sqrt{2}\pi d_0 \sqrt{1 + \frac{3\mu_0}{\sqrt{\rho_0 \gamma d_0}}}. \tag{5}$$

The droplet spacing and the continuity equation for incompressible liquid flow together yield the expected droplet diameter, given by:

$$d_{\text{drop}} = \sqrt{3d_0^2 \lambda/2} \tag{6}$$

For isopropanol, the liquid properties and consequent optimal frequency, spacing, and drop diameter for a 1.4 mL/min flow rate are given in Table 1. The Ohnesorge number, defined as

$$Oh = \frac{\mu}{\sqrt{\rho \sigma L}}, \tag{7}$$

relates the magnitudes of the viscous forces on the drops to the inertial and surface tension forces and which has been used to characterize droplet breakup regimes in past studies.

The light source for the DIH is a Thorlabs L638P200 laser diode with a wavelength of 638 nm, driven by a PicoLas LDP-V 50-100 V3.3 current controller and pointed in the -Z direction. This laser diode was chosen to generate light with high spatial coherence but low temporal coherence, a combination which has been found to be well-suited for holography applications [9]. The current controller is connected to a pulse-delay generator to control pulse width and delay so that the laser pulse falls within the open gate of the high-speed camera (Phantom v2512). The laser beam is collimated through a 2"-diameter convex lens. The L638P200 laser diode is driven, for holography experiments, with a

Density (kg/m^3)	786
Viscosity (kg/(m s))	2.4E-3
Surface Tension γ (N/m)	0.023
Optimal Frequency (Hz)	3601
Droplet Spacing (m)	5.73E-4
Droplet Diameter (m)	2.31E-4
Ohnesorge Number (Oh)	3.714E-3

Table 1 Table 1: Liquid and Drop Properties for Isopropanol at a 1.4 mL/min flow rate

[8]

pulse width of 75 ns at a frequency of 100,000 Hz. Photodetector response to show the pulse shape are shown in Fig. 2. The standard deviation of the pulse intensity is less than 2%.

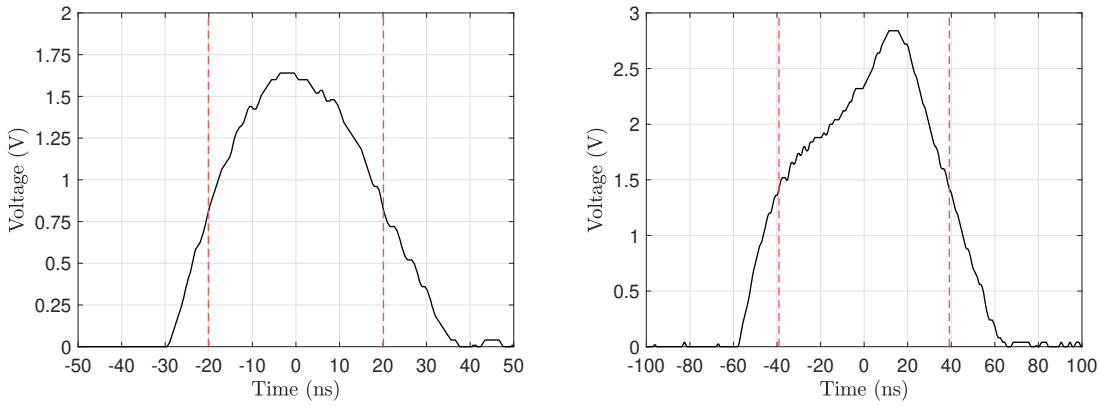

Fig. 2 Single Pulse Photodetector Measurement for 40 ns pulse, left, and 75 ns pulse, right.

The holograms produced by interaction of the isopropanol droplets with the incoming laser light are recorded by a Phantom v2512 high-speed camera. The camera is operated at a frequency of 100,000 frames per second, and uses a 512x384 pixel sensor with a pixel center-to-center spacing of 28 microns. The camera serves as a trigger for the laser diode to ensure that the image is illuminated at every frame. An air hose with a converging nozzle attachment was used to generate air jets to study droplet deformation and aerobreakup behavior. This hose was maintained at 20 psig.

IV. Raw Holograms

Raw holograms were generated in experiments involving free vertical droplet fall and free vertical droplet fall disrupted by an air jet pointing in the +X direction or at a 33.2° angle to the +X direction. Fig. 3 shows a stream of droplets falling vertically without jet disruption, a similar stream disrupted by an air jet, and an air jet deflected by a piece of metal angled at 33.2°. The last flow field is used to study the setup's capability of working near the surface of another body. Each hologram is inverted–the droplets fall toward the top side of each image.

In each image, the hologram produced by a droplet is visible as a series of concentric dark rings around a central light Rayleigh spot. Immediately, one can see the impact of the air jets on the droplet flow. Fig. 3 (center), showing the drop stream disrupted by an air jet normal to the vertical axis, shows significant droplet surface disruption. The breakup behavior seems, qualitatively, to match the bag or multi-bag breakup behavior documented, respectively, by Reinecke and Waldman [10] and Theofanous and Li [11]. The Ohnesorge number for these drops, 0.003714, is close to that of the drops studied by Theofanous and Li [11], which was 0.013. The Weber number, which can be between 1e4 and 1e6 depending on the exact velocity of the air jet, is also in the same range studied by Reinecke and Waldman [10].

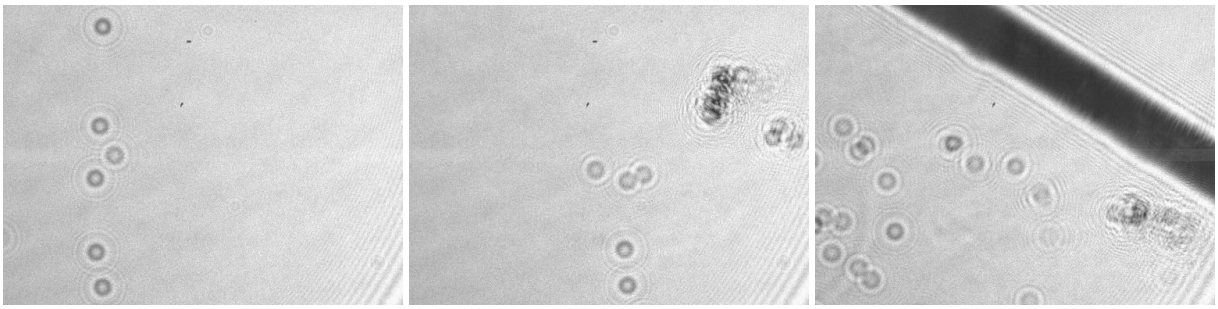

Fig. 3 Hologram produced by isopropanol droplets flowing at 1.4 mL/min and subjected to a 3600 Hz disturbance in the droplet generator. Left: free fall, no disturbance, Center: jet flow, Right: an air jet deflected by a plate at a 33.2°angle

V. Processed Holograms

Each hologram frame is first normalized by an average image generated for each video recorded by the high-speed camera. This reduces noise produced by dust on the camera window or diffraction around the edges of the collimation lens or camera aperture.

After normalization by the average holographic picture for each video, each frame of the holographic videos is subjected to the hybrid method described by Gao and Guildenbecher. In this method, maps of the minimum intensity, maximum Tenengrad operator, and Tenengrad depth for each frame are constructed as functions of iterated values of distance between the camera and the object (henceforth referred to as "z-distance" for brevity). The equations for each of these three maps are given by

$$I_{\min}(x, y) = \min_{z} I_r(x, y, z), \tag{8}$$

$$T_{\max}(x, y) = \max_{z} T(x, y, z), \tag{9}$$

and

$$D_T(x, y) = \arg\left(\max_{z} T(x, y, z)\right). \tag{10}$$

The Tenengrad operator quantifies the sharpness of a reconstructed image and is given by

$$T(x, y, z) = [A_r(x, y, z) \otimes S_x]^2 + [A_r(x, y, z) \otimes S_y]^2, \tag{11}$$

where S_x and S_y are Sobel kernels, A_r is the reconstructed amplitude for a given z-distance, and x and y are coordinates in the image. For example, Fig. 4 shows the minimum intensity map and maximum Tenengrad map for the hologram presented in Fig. 3 (left). A depth range from 19 cm to 23 cm is selected, since the z-distance between the camera charge-couple device (CCD) and the droplet dispenser is approximately 21.5 cm.

The second step in this method of hologram reconstruction is image segmentation using an image amplitude threshold of 0.75. That is, contiguous regions where the image amplitude is less than or equal to 0.75 times the maximum amplitude are considered discrete particles. Rectangular local windows are defined around each detected particle, with a size approximately twice that of the enclosed particle. Within each window, a local optimal amplitude threshold is identified by maximizing the local sharpness $S_W(t)$ given by

$$S_W(t) = \frac{\sum_{x,y \in W} (\xi(\mathscr{T}_t(I_{\min})) \cdot T_{\max}}{\sum_{x,y \in W} (\xi(\mathscr{T}_t(I_{\min}))}, \tag{12}$$

where $\mathscr{T}$ denotes the thresholding operation, and the symbol ξ denotes the edge-finding operation. A value for the local threshold, t, which maximizes image sharpness is chosen. This process is locally repeated after the hologram is reconstructed, using the local intensity rather than the global intensity, to further refine particle detection.

Fig. 5, 6, and 7 give the reconstructed images generated by the HoloSand tool for each of the three holographic videos at frames 1, 21, 41, 61, 81, and 101–that is, at times separated by 0.2 milliseconds. The identified drops are outlined and

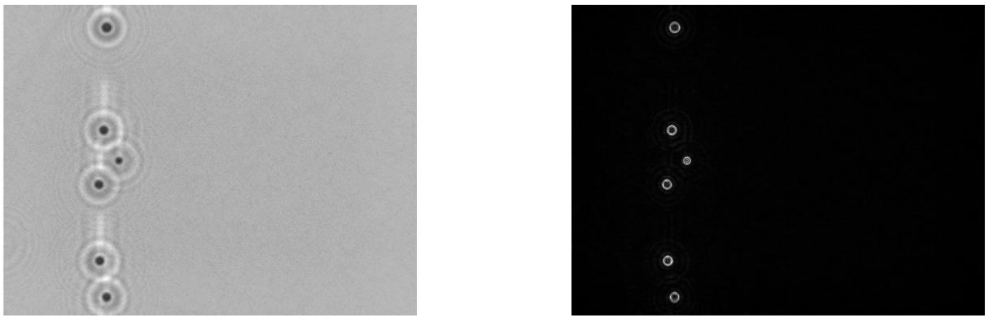

Fig. 4 Left: Minimum Intensity Map for Free-Falling Isopropanol Drops Hologram. Right: Maximum Tenengrad Map for Free-Falling Isopropanol Drops Hologram

colored according to their calculated diameter. In Fig. 7, from the experiment with an angled metal plate, the plate itself has dropped out of the hologram as a result of the normalization process. The effects of aerobreakup on the droplet streams are readily apparent. Drops disrupted by the wind stream are substantially elongated, and then flatten out in the plane normal to the air jet. This is characteristic of the bag breakup observed by Reinecke and Waldman [10] and Theofanous and Li [11]. The breakup behavior in the angled images, in Fig. 7, is similar, and produces a large number of much smaller (diameter < 100 microns) droplets.

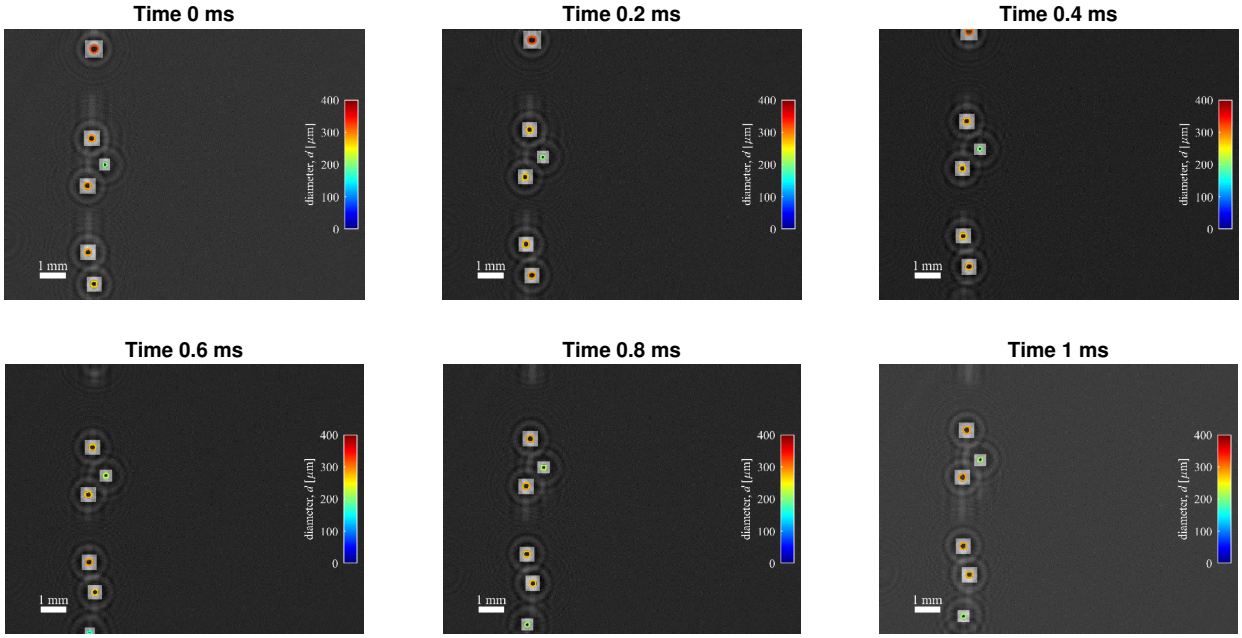

Fig. 5 Reconstructed holograms for six frames from free-falling drops video

The calculated drop diameters in Figs. 5, 6, and 7 are in agreement with the calculated diameter of isopropanol droplets produced through amplification of surface perturbations (that is, 231 microns, as in Table 1). In Fig. 5, the average diameter of the undisturbed isopropanol drops is 268 microns, which is some 5-16% greater than that predicted by Eqs. 5-6.

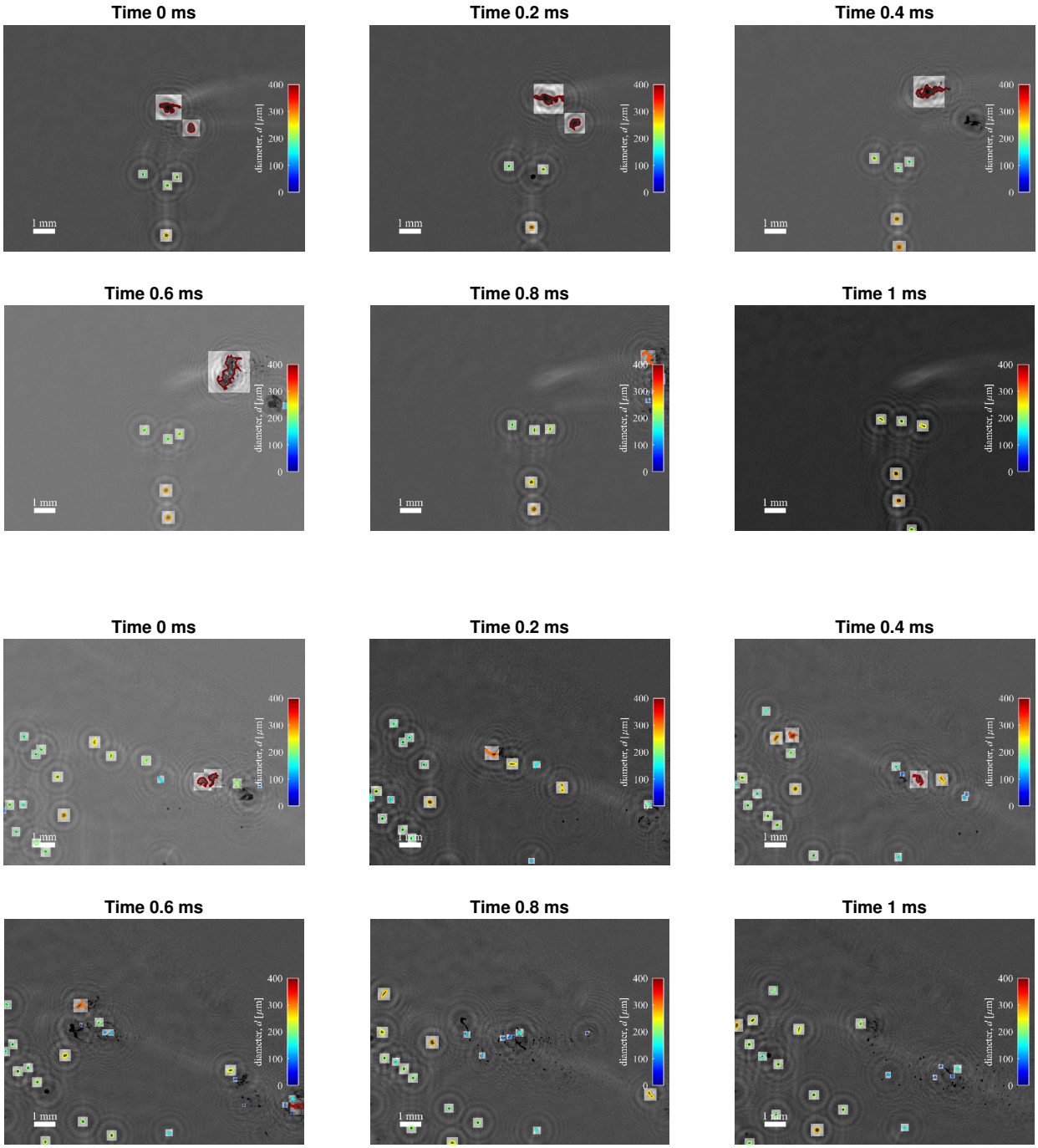

Fig. 7 Reconstructed holograms for six frames from drops with deflected jet disturbance video

VI. Particle Tracking

Between certain consecutive frames, identified particles can 'drop out,' that is, not be identified by the HoloSand tool. For example, it is visible in Fig. 6 that, at time T0+0.2 ms, one of the drops in the middle of the image is not identified by HoloSand. It is, however, identified at times T0 and T0+0.4 ms, and in the consecutive frames around time

T0+0.2 ms. In order to resolve this issue, a particle tracking algorithm was implemented in order to identify particles in non-consecutive image frames and trace their movement between them.

The particle tracking algorithm implemented for this study was that developed by Tinevez [12]. This algorithm, a Hungarian routine match-probability method, identifies for every particle in a given frame a corresponding 'source' (in earlier frames) or 'target' (in later frames) particle. It achieves this by minimizing the sum of all pair distances between any two frames. If a particle track is found to terminate near the start of another track, a link can be created between the two tracks.

The particle tracking algorithm was applied to all three videos used in this study. 2D particle tracks for each video are presented in Figs. 8, 9, and 10. Each figure presents an X-Y view (drops from above, jet from the left, laser propagation toward the viewer) and an X-Z view (laser propagation from above, drops into the page, jet from the left). In each figure, the particle tracks begin where the particle is first detected by the combination of HoloSand and the particle tracking algorithm and end when either the particle no longer exists or the video ends. In Fig. 8, the particles all follow a straight course down and slightly to the left in the image. No particle breakup is noted, or was expected, for this experiment. In Fig. 9, the observed drops begin interacting with the air jet about halfway down the image. Drops in this area break up into smaller drops, whose tracks are much shorter because of the greater difficulty in distinguishing them from their neighbors and because of ongoing drop breakup. 131 different droplets are detected during the millisecond that the holographic video is recorded. Two of the large drops (whose tracks are colored blue and green) are seen to descend into the air jet and become entrained in it, but the video ends before they break up. In Fig. 10, 392 separate particles are detected over the entire millisecond that holographic video is recorded.

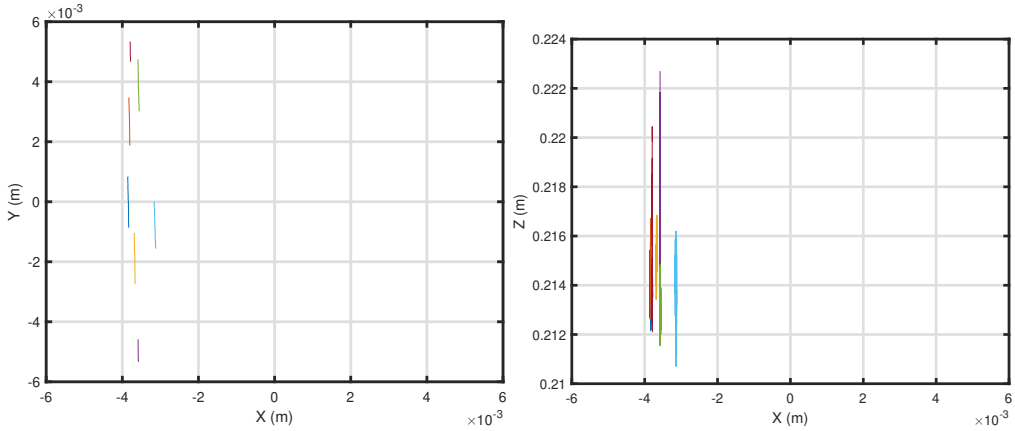

Fig. 8 Particle Tracks for isopropanol drops falling into quiescent air. Left: XY plane, drops falling from top. Right: XZ plane, drops falling into page, laser propagation from top of page

As the XZ-plane images (Figs. 8-10, right) show, the calculated z-distance for all the particles is much more consistent for particles near the center of the hologram. For the freely-falling drops (Figure 8, right), the calculated z-distance varies by up to +/- 1 mm near the center of the hologram but up to +/- 5 mm near the edges. For the drops deflected by the normal air jet (Fig. 9, right), calculated z-distance varies by up to +/- 2 mm near the center of the hologram, where the air jet is disrupting drop shapes.

VII. Conclusion

A digital holography apparatus was constructed using a droplet microdispenser, syringe pump, function generator, high-speed camera, and the novel application of a laser diode to produce coherent light. This apparatus was used to produce isopropanol droplets of uniform spacing and separation through amplified surface perturbations. Holograms of these droplets were generated as they fell through quiescent air or were disturbed by a jet of air applied either horizontally or when deflected by a metal plate. These holograms were processed using the HoloSand suite of tools produced by Sandia National Laboratory and droplet distances from the camera CCD sensor and droplet diameters were measured. A particle tracking algorithm was incorporated into the research effort in order to account for identified drops that were lost between consecutive holographic video frames.

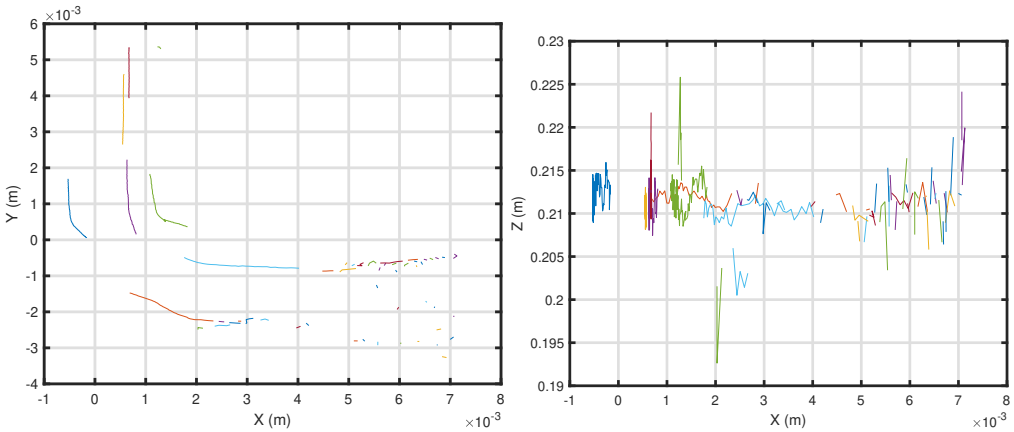

Fig. 9 Particle Tracks for isopropanol drops deflected by normal air jet. Left: XY plane, jet from left, drops falling from top. Right: XZ plane, jet from left, drops falling into page, laser propagation from top of page

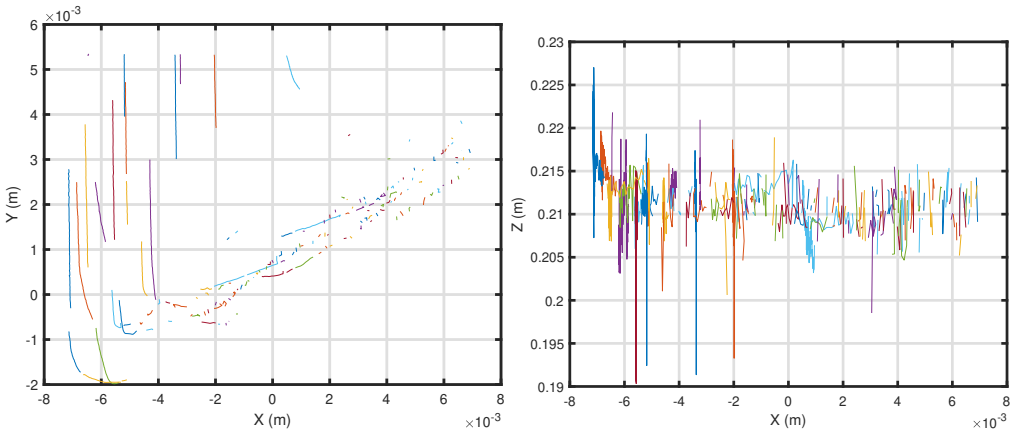

Fig. 10 Particle Tracks for isopropanol drops deflected by angled air jet. Left: XY plane, jet from left, drops falling from top. Right: XZ plane, jet from left, drops falling into page, laser propagation from top of page

Acknowledgments

Dworzanczyk and Parziale were supported by ONR-MURI Grant N00014-20-1-2682. **Special thanks** go out to Dr. Daniel Guildenbecher for his invaluable assistance in troubleshooting the use of the HoloSand program, and to Mr. David Schektman and Mr. Ahsan Hameed of Stevens Institute of Technology for their assistance in setting up and operating the laser illumination apparatus.

References

[1] Katz, J., and Sheng, J., "Applications of Holography in Fluid Mechanics and Particle Dynamics," *Annual Review of Fluid Mechanics*, Vol. 42, 2010, pp. 531–555. doi: 10.1146/annurev-fluid-121108-145508.

[2] Gao, J., Guildenbecher, D. R., Reu, P. L., and Chen, J., "Uncertainty characterization of particle depth measurement using digital in-line holography and the hybrid method," *Optics Express*, Vol. 21, No. 22, 2013. doi: 10.1364/OE.21.026432.

[3] Guildenbecher, D. R., Gao, J., Reu, P. L., and Chen, J., "Digital holography simulations and experiments to quantify the accuracy of 3D particle location and 2D sizing using a proposed hybrid method," *Applied Optics*, Vol. 52, No. 16, 2013, pp. 3790–3801.

[4] Guildenbecher, D., "Sandia Particle Holography Processor v. 1.0, Version 00," , 2015. URL https://www.osti.gov/biblio/1242887.

[5] Guildenbecher, D. R., Cooper, M. A., and Sojka, P. E., "High-speed (20 kHz) digital in-line holography for transient particle tracking and sizing in multiphase flows," *Applied Optics*, Vol. 55, 2016, pp. 2892–2903. doi: 10.1364/AO.55.002892.

[6] Reinecke, W. G., and McKay, W. L., "Experiments on Water Drop Breakup Behind Mach 3 to 12 Shocks," SC-CR-70-6063, 1969.

[7] Shimasaki, S., and Taniguchi, S., "Formation of uniformly sized metal droplets from a capillary jet by electromagnetic force," *Applied Mathematical Modeling*, Vol. 35, 2011, pp. 1571–1580.

[8] PubChem, "Isopropyl Alcohol," , 2021. https://pubchem.ncbi.nlm.nih.gov/compound/Isopropyl-alcohol,accessed 2021-5-15.

[9] Deng, Y., and Chu, D., "Coherence properties of different light sources and their effect on the image sharpness and speckle of holographic displays," *Scientific Reports*, 2017. doi: 10.1038/s41598-017-06215-x.

[10] Reinecke, W. G., and Waldman, G. D., "A Study of Drop Breakup Behind Strong Shocks with Applications to Flight," AVSD-0110-70-RR, 1970.

[11] Theofanous, T. G., and Li, G. J., "On the physics of aerobreakup," *Physics of Fluids*, Vol. 20, No. 5, 2008, p. 052103. doi: 10.1063/1.2907989.

[12] Tinevez, J., "simpletracker," , 2019. URL {https://www.github.com/tinevez/simpletracker},accessed2021-6-21.